High quality, low oxygen content and biocompatible graphene nanosheets obtained by anodic exfoliation of different graphite types

J.M. Munuera[a*], J.I. Paredes[a], S. Villar-Rodil[a], M. Ayán-Varela[a], A. Pagán[b], S.D. Aznar-Cervantes[b], J.L. Cenis[b], A. Martínez-Alonso[a], J.M.D. Tascón[a]

[a]*Instituto Nacional del Carbón, INCAR-CSIC, Apartado 73, 33080 Oviedo, Spain*

[b]*Instituto Murciano de Investigación y Desarrollo Agrario y Alimentario (IMIDA), C/Mayor 1, 30150 La Alberca (Murcia), Spain*

[*]Corresponding author. Tel: (+34) 985 11 90 90. E-mail: j.munuera@incar.csic.es (J.M: Munuera)

Abstract

Anodic exfoliation of graphite has emerged as an attractive method to access graphene nanosheets in large quantities, but oxidation reactions associated to this process compromise the structural quality of the resulting materials. Here, we demonstrate that the type of starting graphite material impacts the oxygen and defect content of anodically exfoliated graphenes obtained thereof. We investigated highly oriented pyrolytic graphite (HOPG) as well as graphite foil, flakes and powder as electrode in the anodic process. Importantly, materials with low levels of oxidation and disorder (similar to those typically achieved with cathodic exfoliation approaches) could be attained through proper choice of the graphite electrode. Specifically, using graphite foil afforded nanosheets of higher quality than that of HOPG-derived nanosheets. This discrepancy was interpreted to arise from the structural peculiarities of the former, where the presence of folds, voids and wrinkles would make its exfoliation process to be less reliant on oxidation reactions. Furthermore, cell viability tests carried out with murine fibroblasts on thin graphene films suggested that the anodically exfoliated graphenes investigated here (possessing low or high oxidation levels) are highly biocompatible. Overall, control upon the extent of oxidation and disorder should expand the scope of anodically exfoliated graphenes in prospective applications.

1. Introduction

More than ten years after it could be first isolated by a relatively straightforward exfoliation approach [1], graphene has become one of the most intensively studied objects from the condensed matter physics and materials science fields [2–4]. Although research efforts were originally focused for the most part on purely fundamental aspects related to the exceptional electronic, mechanical, thermal and optical properties of this two-dimensional carbon structure, more recent years have witnessed a shift in emphasis towards its implementation in a wide variety of relevant target applications [4]. However, fulfilling the promise of graphene as a disruptive material in real-life applications will first and foremost require its large-scale production by methods that should ideally be simple, inexpensive and versatile enough to afford products with characteristics tailored to each intended use. Because no single method known to date can deliver cost-effective graphene materials with high yields and on-demand characteristics at the same time, researchers have directed their efforts towards the development of a pool of bottom-up and top-down fabrication approaches, each of which exhibits its own advantages and drawbacks and is therefore best suited to certain applications [4,5].

Bottom-up production methods are dominated by chemical vapor deposition (CVD) of hydrocarbons onto suitable metal substrates (e.g., copper), which gives access to high quality graphene wafers appropriate for applications in electronics and photonics [5,6]. Unfortunately, issues related to the use of high temperatures and a sacrificial metal or the need of subsequent transfer processes hamper its widespread adoption. Among top-down methods, which are based on the exfoliation of graphite and graphite derivatives [7,8], the so-called graphite oxide route has received a great deal of attention, as it can provide single-layer sheets of graphene oxide (GO) and reduced graphene oxide (RGO)

with high throughput and yield [9,10]. Nevertheless, the obtained materials are typically very defective; as a result, many of the attractive physical properties observed in pristine graphene have been found to degrade in GO/RGO [11]. While full structural restoration of the latter has been shown to be feasible, the process relies on the use of very high temperatures (>1500 ºC), making it impractical for most applications [12,13]. Alternatively, defect-free graphene flakes can be procured by direct exfoliation of graphite in the liquid phase, usually with the assistance of ultrasound or shear forces [14–16]. This method readily lends itself to the preparation of colloidal graphene dispersions that can be further processed into useful materials, such as thin films, composites or hybrids, but usually suffers from low yields and relatively limited exfoliation degrees (multilayer graphene), as well as small flake sizes.

Another top-down approach to graphene production that has emerged in recent years is the one based on electrochemical exfoliation of graphite, which boasts such appealing features as simplicity and speed of operation or a strong potential to be scaled-up [17–19]. Although a variety of electrochemical processes have been successfully tested towards this end [19], they can be broadly classified into either (1) cathodic exfoliation in organic solvents (propylene carbonate, dimethyl sulfoxide, etc) containing lithium or alkylammonium salts as the electrolyte [20–24], or in water in some specific cases [25] or (2) anodic exfoliation in ionic liquid-water mixtures or aqueous solutions of acids (mainly H_2SO_4) or inorganic salts [26–33]. The anodic exfoliation protocols are particularly attractive due to their greener character (use of water/ionic liquids vs. organic solvents) and generally higher and faster production rates. However, contrary to the case of cathodic exfoliation, the obtained graphene materials tend to be decorated with significant amounts of oxygen functional groups that compromise their structural quality [25,28–33]. Such functionalization is thought to be the result of oxidation

processes inherent to the application of anodic potentials to the graphite electrode. To alleviate this problem, some researchers have proposed using aqueous solutions of inorganic salts instead of acids as the electrolyte (e.g., K_2SO_4 rather than H_2SO_4) [28,31], but the data available in the literature still reveal a wide variability in oxygen content for anodically exfoliated graphenes prepared through such a strategy [31,33,34].

In addition to the electrolyte nature, we hypothesize that other factors such as the type of graphite used for exfoliation could be critical in determining the oxygen content, and thus the structural quality, of anodically derived graphenes. It is well-known in carbon science that oxidation and intercalation of graphitic materials, the two main processes that are thought to drive anodic exfoliation [27,31], are greatly dependent on their specific microstructure (particle/grain size, presence of imperfections, etc) [35,36]. Consequently, graphene materials with different characteristics and thus a variety of potential uses should be expected when different graphite types are employed, but to the best of our knowledge this question has not yet been studied and elucidated, let alone taken advantage of. In the present work, we address this issue by investigating the anodic exfoliation of several different types of graphite to give graphene nanosheets. The results indicate that the oxygen and defect contents of such graphenes are highly dependent on graphite type, which could be mainly attributed to their morphological peculiarities. More importantly, graphenes with minimized content of oxygen and structural defects can be obtained through judicious choice of the starting graphite. Finally, materials based on anodically exfoliated graphenes could be promising for biomedical applications, but their biocompatibility has not yet been investigated. Hence, we also report here cell proliferation tests on thin films of anodically exfoliated graphenes of different characteristics towards the murine fibroblast cell line L-929, which suggest these types of graphene to be highly biocompatible.

2. Experimental

2.1. Preparation of graphene by anodic exfoliation of different graphite types

Four different types of graphite were used in the present study: highly oriented pyrolytic graphite (HOPG; grade ZYH, obtained from Advanced Ceramics), graphite foil (Papyex I980, obtained from Mersen), natural graphite flakes (ref. 332461, from Sigma-Aldrich) and natural graphite powder (grade 2910, from Mersen). For the electrochemical exfoliation experiments, ~10×10×2 mm^3 pieces of HOPG and graphite foil were employed, whereas the graphite powder and flake materials were pressed into circular pellets (12 mm in diameter, 2 mm in thickness) by means of a hydraulic press. Exfoliation was conducted in a two-electrode system by immersing a graphite piece/pellet and a Pt wire into an aqueous 0.1 M K_2SO_4 solution, which were used as working and counter electrodes, respectively. The Pt wire was placed parallel to the graphite sample at a distance of about 2 cm. Then, a positive voltage (10 V, 0.5 A) was applied to the graphite electrode using a DC power supply (Agilent 6614C apparatus) for periods of time that typically ranged between a few and several minutes. Such a process led to the continuous expansion and detachment of graphite fragments from their parent piece/pellet, which tended to float on the electrolyte solution. This expanded product was then collected, thoroughly rinsed off with copious amounts of Milli-Q water to remove residual salts and dried overnight at room temperature under reduced pressure. Colloidal dispersions of the resulting expanded materials, either in water assisted by flavin mononucleotide (FMN) as an efficient stabilizer or in *N*,*N*-dimethylformamide (DMF), were obtained either through bath sonication (Selecta Ultrasons system, 40 kHz) or, alternatively, by shear mixing (IKA T-25 Ultra-Turrax high-speed homogenizer; rotor diameter: 12.7 mm; rotor-stator gap: 300 μm; rotor

speed: 9000 rpm) for 1 h, followed by centrifugation at 200 *g* for 20 min (Eppendorf 5424 microcentrifuge) to sediment the non fully exfoliated or poorly exfoliated graphite fraction. Finally, the top ~75% of the obtained supernatant was collected and stored for further use. In the case of the FMN-stabilized aqueous dispersions, this supernatant was further subjected to two cycles of sedimentation (20000 *g*, 20 min) and resuspension in Milli-Q water to remove the free (non-adsorbed) FMN fraction.

2.2. Characterization techniques

Characterization of the anodically exfoliated graphenes was carried out by UV-vis absorption spectroscopy, field-emission scanning electron microscopy (FE-SEM), atomic force microscopy (AFM), X-ray photoelectron spectroscopy (XPS), attenuated total reflection Fourier transform infrared (ATR-FTIR) spectroscopy, Raman spectroscopy as well as electrical conductivity measurements. UV-vis absorption spectra were recorded with a double-beam Heλios α spectrophotometer (Thermo Spectronic). FE-SEM images were acquired on a Quanta FEG 650 microscope (FEI Company) at 25 kV. AFM imaging was accomplished with a Nanoscope IIIa Multimode apparatus (Veeco) under ambient conditions in the tapping mode of operation, using Si cantilevers with nominal spring constant and resonance frequency of ~40 N m^{-1} and about 250-300 kHz, respectively. Specimens for AFM were prepared by drop-casting colloidal graphene dispersions (~0.1-0.2 mg mL^{-1}) onto pre-heated (50-60 ºC) SiO_2/Si or freshly cleaved HOPG substrates, which were then allowed to dry. XPS measurements were performed on a SPECS system under a pressure of 10^{-7} Pa with a monochromatic Al K_α X-ray source operated at 100 W. ATR-FTIR spectra were obtained with a Nicolet 3700 spectrometer (Thermo Scientific) using diamond as ATR crystal. Raman spectra were recorded on a Horiba Jobin-Yvon LabRam instrument at a

laser excitation wavelength and incident power of 532 nm and 2 mW, respectively. Electrical conductivity measurements were carried out by the van der Pauw method using a home-built setup (Agilent 6614C DC power supply and Fluke 45 digital multimeter). Graphene samples for XPS, ATR-FTIR and Raman spectroscopy, as well as electrical conductivity measurements were prepared in the form of free-standing, paper-like films by vacuum filtration of the corresponding FMN-stabilized aqueous dispersions through either silver or polycarbonate membrane filters 47 mm in diameter and 0.2 μm of pore size (Sterlitech Corporation).

2.3. L-929 cell line viability tests for thin films of anodically exfoliated graphene

The biocompatibility of the anodically exfoliated graphenes was evaluated on the basis of cell proliferation assays carried out on polystyrene culture plates covered by a thin film of the different graphene specimens. Murine fibroblasts (L-929 cell line, ECACC No 85011425) were chosen for these studies, because such a cell type is highly stable, fast-growing and commonly used in cytotoxicity experiments. 48-well tissue culture plates were coated with either ~0.25 or 0.50 mg of each graphene sample by depositing, respectively, 125 or 250 μL of the corresponding FMN-stabilized aqueous dispersion at a concentration of ~2 mg mL^{-1}. Such a procedure led to films with approximate thickness of 1 μm (0.25 mg) and 2 μm (0.50 mg). Following sterilization, the culture plates were incubated only with pure fetal bovine serum (FBS) at 37 ºC for 2 h to facilitate the initial fibroblast adhesion. Then, the FBS was removed and the culture plates were seeded with the L-929 cells at a density of 5000 cells per well. Dulbecco´s modified Eagle´s medium (DMEM) supplemented with 10% FBS, penicillin (100 U mL^{-1}) and streptomycin (100 mg mL^{-1}) was used as culture medium at 37 ºC in a 7.5% CO_2 atmosphere. This medium was carefully replaced twice a week during the cell

growth experiments. Cell proliferation was determined by means of the MTT assay, which is based on the enzymatic reduction of the tetrazolium dye 3-(4,5-dimethylthiazol-2-yl)-2,5-diphenyltetrazolium bromide (MTT) to its corresponding purple formazan. The assays were accomplished 1, 4 and 7 days after cell seeding, each experiment being performed in triplicate. To this end, each well from the seeded culture plates was incubated for 4 h in 500 μL of MTT solution (1 mg mL^{-1}) at 37 ºC under 7.5% CO_2 atmosphere [37]. Then, the MTT solution was removed, 200 μL of dimethyl sulfoxide were added to solubilize the water-insoluble purple formazan crystals formed by reduction of MTT, and the absorbance of the resulting solution was measured with a BMG FLUOstar Galaxy microplate reader (MTX Lab Systems, Inc) at 570 nm as well as 690 nm as the reference wavelength.

3. Results and discussion

3.1. Morphological evolution of different graphite types upon anodic treatment

For our study on the influence of the type of graphite starting material on the characteristics of the graphene obtained from it by electrochemical exfoliation, we applied a positive potential (10 V) to a graphite working electrode in a 0.1 M K_2SO_4 aqueous electrolyte. These specific values were chosen on the basis of very recent studies on the anodic exfoliation of graphite in aqueous solutions of sulfate-based salts [31,38] where such parameters were reported to be optimal for graphite exfoliation. In line with these previous reports [31,33,38], application of such potential to a graphite anode in aqueous electrolyte led to the expansion and detachment of small (up to a few millimetres) fragments of the material. Evidence for such an expansion could be gathered by examining the morphology of these fragments by FE-SEM, with noticeable differences being observed depending on the type of graphite used. Fig. 1a-d shows

representative FE-SEM images of the starting HOPG (a,b) and graphite foil (c,d) samples, both for basal plane (a,c) and edge (i.e., prismatic) plane (b,d) views. As could be expected, the basal surface of HOPG appeared essentially flat and featureless (Fig. 1a). In agreement with previous results for this type of graphite [39], more detailed visualization by AFM (Fig. 2a) confirmed a surface topography made up of atomically flat terraces separated by step edges with heights between ~0.35 nm (corresponding to a monolayer-high step) and several nanometers (a few tens of monolayers). This result indicates that the graphene layers in HOPG are very tightly packed with each other, leaving little room, if any, to such imperfections in its structure as voids, ripples or wrinkles. The edge plane surface of the HOPG pieces tended to exhibit a rather compact and relatively rough morphology (Fig. 1b). The latter can be ultimately ascribed to the fact that the edge terminations in the individual graphene layers are typically ill-defined, with a random/uneven combination of zig-zag and armchair configurations that lend a rough profile, as opposed to the atomically flat surface characteristic of the basal plane [40]. On the other hand, the basal surface of the graphite foil samples was seen to be comprised of a disordered stacking of micrometer-sized graphitic platelets that exhibited many flaws such as folds, overlaps or wrinkles (Fig. 1c), whereas their edge surfaces were apparently rather similar to those observed in the case of HOPG (Fig. 1d). AFM imaging (Fig. 2b) corroborated the topographically rugged nature of this type of graphite (compare the magnitude of the vertical scale in the overlaid line profile with that of HOPG in Fig. 2a). As will be discussed below, such differences in the packing configuration of the graphitic layers between HOPG and graphite foil are believed to lead to anodically exfoliated graphene materials with distinct characteristics.

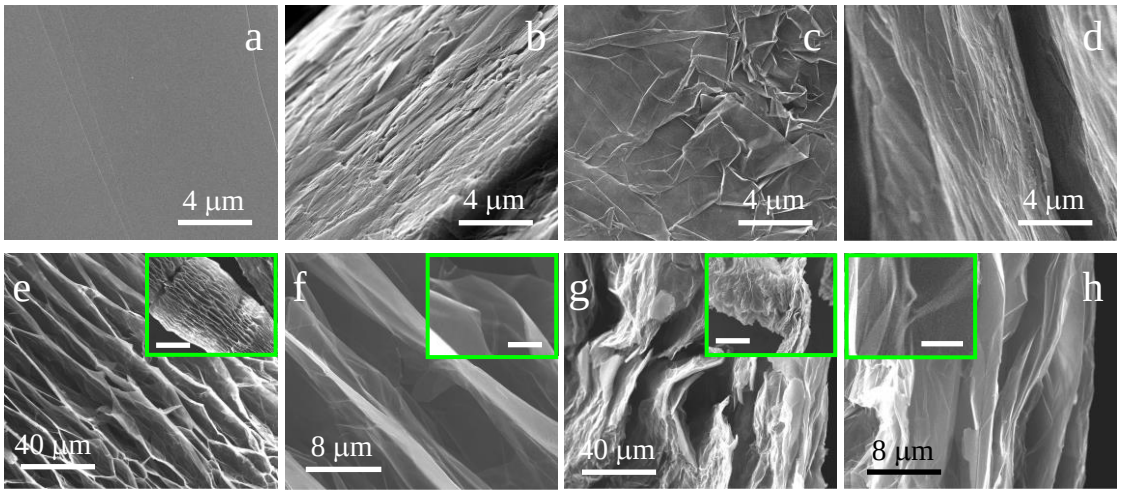

Figure 1. Representative FE-SEM images of the basal (a,c) and edge (b,d) surfaces of the starting HOPG (a,b) and graphite foil (c,d) materials as well as of the edge surfaces of HOPG (e,f) and graphite foil (g,h) after electrochemical exfoliation treatment for 15 min. Scale bars of the inset images: 200 μm (e and g) and 1 μm (f and h).

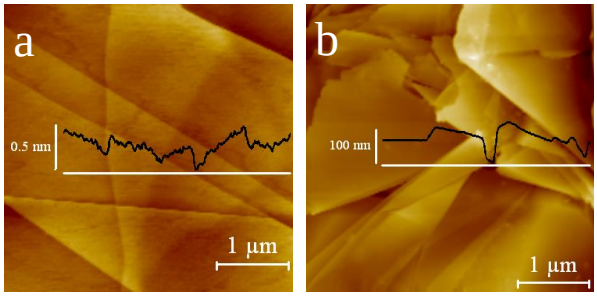

Figure 2. AFM images of the basal surface of the starting HOPG (a) and graphite foil (b) materials. Representative line profiles taken along the marked white lines are shown overlaid on the images.

Following anodic treatment, both the HOPG and graphite foil materials showed evidence of highly expanded structures. Fig. 1e-h presents FE-SEM images of the prismatic surface of detached graphite fragments after 15 min of electrochemical exfoliation for HOPG (e,f) and graphite foil (g,h). The HOPG fragments were frequently found in a more or less uniform, accordion-like expanded form (Fig. 1e and

its inset), with large voids many micrometers wide having developed between the cleaved layers. As noticed from Fig. 1f, this type of structure tended to replicate on smaller length scales, so that higher resolution imaging often revealed thinner layers separated by narrower voids (inset to Fig. 1f). Indeed, FE-SEM inspection at the highest possible magnification disclosed split layers that were at least as thin as a few to several nanometers, indicating that the electrochemical exfoliation process was quite efficient. In the case of the graphite foil samples, the electrochemical expansion led to detached fragments with a much more ill-defined structure on large length scales (Fig. 1g and its inset). We attribute such a result to the particular configuration of this type of graphite discussed above, where the disordered packing of folded and/or wrinkled graphitic platelets would not favor a homogeneous expansion of the layers in an accordion-like fashion similar to that observed for HOPG. Nevertheless, more detailed scrutiny of the expanded structures (Fig. 1h and its inset) indicated that on a local scale very thin layers were effectively separated from one another also in this case, thus suggesting a degree of exfoliation comparable to that attained with the HOPG samples. Further analysis of the exfoliated products by AFM confirmed that this was indeed the case (see below).

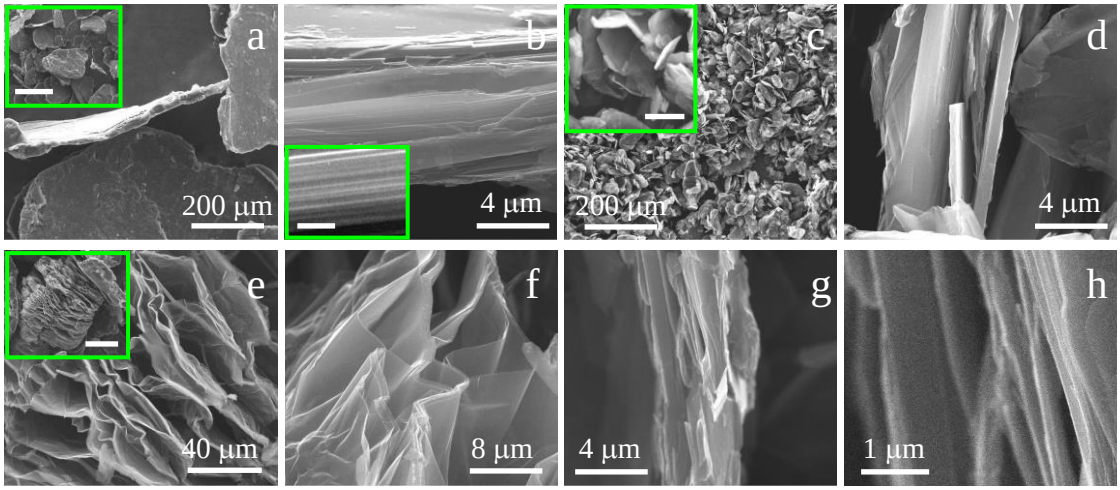

Figure 3. Typical FE-SEM images of the starting graphite flakes (a,b) and powder (c,d), as well as graphite flakes (e,f) and powder (g,h) after electrochemical exfoliation

treatment for 3 min. Scale bars of the inset images: 1 mm (a), 250 nm (b), 20 μm (c) and 200 μm (e).

Fig. 3 shows representative results from the FE-SEM observations carried out for the graphite flake and powder samples. The former material was seen to be comprised of slabs ~10-40 μm thick and typical lateral dimensions between 500 and 1000 μm (Fig. 3a and inset). Edge plane views of these slabs (Fig. 3b and inset) indicated that their graphitic planes were organized in a compact, well ordered fashion. The graphite powder material was made up of much smaller particles (Fig. 3c and inset), with typical thickness and lateral dimensions of about 1-4 and 10-50 μm, respectively, and their graphitic planes displayed a compact arrangement as well (Fig. 3d). For both types of graphite, anodic exfoliation times of 3 min were employed. Due to their small size (especially in the case of the powder samples), the individual graphite particles in the pelletized working electrode tended to expand very quickly during the electrolytic process. This led in turn to the prompt detachment of the particles from the pellet, so that a graphite electrode with a mass comparable to that of the HOPG and graphite foil electrodes used here (~0.5 g) was completely taken apart in 3 min. Such a length of time was sufficient to induce a large, accordion-like expansion of the graphite flakes (Fig. 3e and inset), yielding very thin separated layers (Fig. 3f) similar to those observed for HOPG pieces after 15 min of electrochemical treatment (Fig. 1e and f). Furthermore, we note that the same type of expanded structures was brought about with only 3 min of treatment in HOPG (images not shown). However, the electrochemical expansion was much more limited when using graphite powder (Fig. 3g). In this case, no accordion-like structures were developed and only relatively narrow voids were generated between the thin cleaved layers (Fig. 3h). This result suggests that exfoliation was significantly

less efficient with graphite powder compared to the other three types of graphite. We interpret that, due to their small size, the individual graphite particles that comprise a pellet of the powder material are in contact with neighboring particles only at a relatively limited number of points. Thus, a graphite particle on the surface of the pellet that is expanding as a result of the electrochemical treatment in contact with the electrolyte will rapidly loose (electrical) contact with the pellet, so that its expansion will become arrested at a relatively early stage of the process. Hence, the resulting product can be expected to exhibit a limited extent of expansion, as it was indeed the case (Fig. 3g and h). For pellets with much larger particle sizes (i.e., flakes) or monolithic graphite samples (i.e., the HOPG and graphite foil pieces), the expanding particles/fragments will be in contact with the rest of the electrode for longer times, thus enabling higher degrees of expansion. Support for this interpretation was gathered from the observation that detachment of graphitic fragments/particles from the electrodes proceeded at the slowest pace for the HOPG and graphite foil samples, was somewhat faster when using the flake material, and was the fastest with the graphite powder.

3.2. Processing and characteristics of graphene materials derived from anodically exfoliated graphites

Irrespective of the specific morphologies developed during the anodic treatment, the four types of graphite employed here required an additional processing step to complete the exfoliation process. This is the case with almost all the electrochemical exfoliation methods (both anodic and cathodic) that have been reported to this day, and such a step is usually accomplished via sonication in suitable aqueous or organic solvents to afford stable colloidal dispersions of thin, well-exfoliated graphene flakes [19]. We tested the formation of colloidal graphene suspensions from the anodically expanded products

both in water assisted by the biomolecule FMN and in the organic solvent DMF. The latter is well known to efficiently stabilize pristine as well as graphite oxide-derived graphene flakes [41−43], whereas FMN, a phosphorylated derivative of riboflavin (vitamin B_2), has been identified as a particularly efficient dispersant of graphene flakes in aqueous medium, delivering high flake concentrations at low FMN/graphene mass ratios [44,45]. The anodically expanded graphites were subjected either to sonication in an ultrasound bath cleaner or to shear mixing in a high speed homogenizer (see Experimental section). We note that shear mixing has been recently put forward as a competitive alternative to sonication in the exfoliation of graphite particles to yield graphene flakes [16,46], but to the best of our knowledge it has not yet been used for the dispersion of electrochemically exfoliated samples.

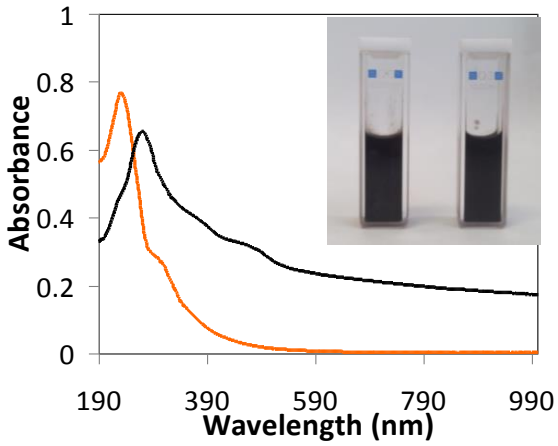

Figure 4. Typical UV-vis absorption spectra of anodically exfoliated graphene dispersed in water with the assistance of FMN as a stabilizer (black trace) and unreduced GO, also dispersed in water (orange trace). Inset: digital photograph of colloidal dispersions of anodically exfoliated graphene derived from graphite foil in water-FMN solution (left cuvette) and DMF (right cuvette).

In our case, both sonication and shear mixing led to the attainment of opaque black dispersions (following a centrifugation step to sediment insufficiently exfoliated fractions) with the four graphite types employed here, and both in FMN/water solution and in DMF. Such dispersions remained visually homogeneous and colloidally stable at least for several weeks, if not months. Two examples of such dispersions (for anodically exfoliated graphite foil after sonication in DMF and FMN/water) are given in Fig. 4 (inset). From UV-vis absorption measurements [45], concentrations of suspended graphitic material between a few tenths of milligram and a few milligrams per milliliter were readily achieved. Fig. 4 (black trace) shows an UV-vis absorption spectrum that was representative of those recorded for the water-based suspensions regardless of graphite type and dispersion method used. All the spectra were dominated by an absorption peak located at ~268-270 nm and strong absorbance in the whole wavelength range above 270 nm, along with two weak shoulders at about 370 and 450 nm. The former two features are known to be characteristic of graphitic, sp^2-based carbon structures [47,48], suggesting the presence of well-exfoliated products in the aqueous medium, whereas the weak shoulders can be attributed to the stabilizing FMN molecules adsorbed onto the graphitic materials [45]. More specifically, the peak at 268-270 nm can be ascribed to $\pi \rightarrow \pi^*$ transitions from electronically conjugated domains in carbon materials [47–49]. The actual position of such a peak is dependent on the size of the conjugated domains (provided that they are of nanometer-sized dimensions), so that a blue-shift in peak position can be expected for domains of decreasing size as a result of quantum confinement effects [49]. This point is relevant for the present anodically exfoliated materials, because the anodic process tends to oxidize the resulting graphene flakes to some extent [19]. For instance, if the graphene lattice became very heavily oxidized, we would expect its structure to contain only tiny

conjugated domains, similar to those observed in, e.g., GO sheets prepared by harsh oxidation of graphite in acidic medium [50]. For comparison purposes, the typical UV-vis absorption spectrum of the latter is given in Fig. 4 (orange trace), its absorption peak being located at ~231 nm. From absorbance data taken from the literature [51,52], the peak position at 268-270 nm measured here for all the electrochemically exfoliated materials would be consistent with graphene flakes having oxygen contents similar to or lower than those of well reduced GO samples. As will be shown below, the XPS results were consistent with this conclusion.

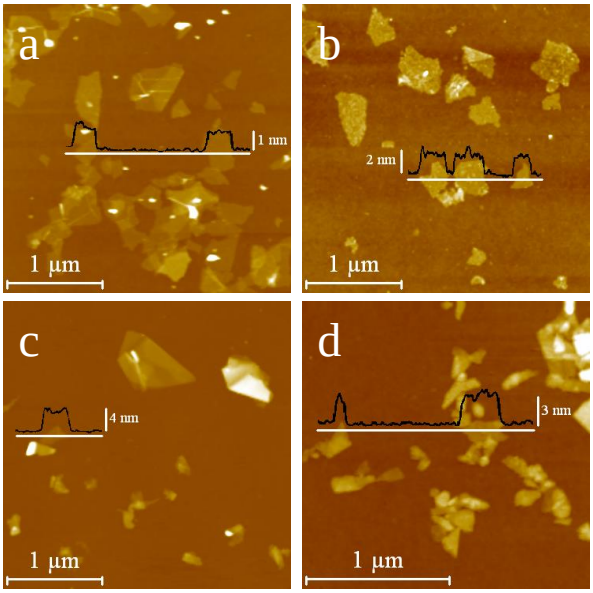

Figure 5. AFM images of anodically exfoliated graphenes obtained from HOPG (a) as well as graphite foil (b), flakes (c) and powder (d). A typical line profile taken along the marked white line is shown superimposed on each image.

The exfoliation degree and lateral size of the graphitic products present in the final colloidal suspensions (i.e., after electrochemical expansion and sonication-/shear mixing-assisted dispersion) was investigated by AFM. Fig. 5 shows typical height images recorded for dispersions derived from HOPG (a) as well as from graphite foil

(b), flakes (c) and powder (d), which were drop-cast onto SiO_2/Si substrates. It was observed that both HOPG and graphite foil afforded very thin nanosheets or platelets with lateral dimensions in the 200-600 nm range and apparent thickness mostly between 1 and 2 nm (see representative line profiles overlaid on the AFM images). Considering that AFM measurements of thickness for both pristine and oxidized forms of graphene supported onto SiO_2/Si generally include an artifactual contribution amounting to ~1 nm [53,54], we conclude that the actual thickness of the sheets obtained from HOPG and graphite foil is not greater than about 1 nm, i.e., the sheets comprise no more than three or four monolayers. We note that such a high extent of exfoliation was attained irrespective of treatment time in the electrochemical expansion step. For example, the AFM image of Fig. 5a corresponds to a treatment time of the HOPG piece of 15 min, but the same results were obtained for 3 and 60 min of electrolytic treatment (images not shown). On the other hand, the graphene platelets derived from graphite flakes and powder (Fig. 5c and d, respectively) tended to be somewhat smaller and thicker. In both cases, their lateral dimensions were between 100 and 400 nm, although larger platelets (up to about 1μm) were occasionally observed, with apparent thickness values mostly in the ~3-4 nm range (for powder) and ~4-5 nm range (for flakes), implying that the exfoliated products were made up of several (typically 6-12) monolayers, even though thicker objects (up to 10-15 nm) were also sometimes present. The typical lateral size and apparent thickness values for the graphene nanosheets obtained from the different graphite types are collected in Table 1.

Because the exfoliated products obtained in the final colloidal dispersions had undergone a sonication/shear-mixing step in addition to the electrolytic process, and the former is known to directly induce the cleavage of graphite to give graphene platelets by itself [14–16], the actual role of the electrochemical treatment in attaining an effective

exfoliation was a priori unclear. To address this issue, as a control experiment the different as-received graphites (i.e., those without prior electrochemical expansion) were subjected to the same sonication procedure as that applied to the anodically expanded materials. For HOPG and graphite foil, hardly any material could be exfoliated and dispersed in the liquid phase, and the exfoliated objects were much thicker than 1-3 monolayers, implying that the electrolysis step was critical in the exfoliation process. For graphite flakes and powder the amount of exfoliated material was significant, but estimated to be only about 1/8 of that achieved when the electrochemical expansion step was included, which indicates that such a step was still the main driving force towards exfoliation. However, the apparent thickness of the sonicated-only platelets was mostly ~5-6 nm, compared with ~3-5 nm measured for products with prior electrochemical expansion, suggesting that electrolysis did not have a very strong effect on the exfoliation degree of platelets derived from these two graphite types.

Table 1. Characteristics of anodically exfoliated graphenes obtained from different types of graphite. For each graphene material, the anodic exfoliation time of the corresponding graphite is given in parenthesis.

Graphene material	Lateral size (AFM) (nm)	Apparent thickness (AFM) (nm)	O/C atomic ratio (XPS)	I_D/I_G (Raman)	Electrical conductivity (S m^{-1})
Graphite powder (3 min)	100-400	3-4	0.041	0.21	22100
Graphite flakes (3 min)	100-400	4-5	0.068	0.11	57200
Graphite foil (15 min)	200-600	1-2	0.058	0.38	13300
Graphite foil (60 min)	200-600	1-2	0.110	0.82	10300
HOPG (3 min)	200-600	1-2	0.055	0.17	7590
HOPG	200-600	1-2	0.091	1.35	4130

(15 min)					
HOPG (60 min)	200-600	1-2	0.180	1.23	7910

As mentioned previously, anodic exfoliation of graphite generally leads to oxidation of the resulting graphene materials. Because oxidation can seriously compromise the performance of many graphene-based materials and devices [55], it is important to develop an understanding of the different factors that have a bearing on such a process. To elucidate the possible effects of graphite type and electrolysis time on oxidation, the chemical composition and nature of functional groups present in the different exfoliated products were analyzed by XPS and ATR-FTIR spectroscopy. Fig. 6a,b shows two illustrative XPS survey spectra, corresponding to graphene platelets derived from (a) HOPG (60 min of electrochemical treatment) and (b) graphite powder (3 min of electrochemical treatment). As could be expected, although carbon was the dominant element in all the samples (C 1s peak located at ~285 eV), oxygen was also present to a significant extent (O 1s peak at ~532 eV). However, the amount of oxygen was also seen to differ considerably between the different samples, as can be noticed from their corresponding O/C atomic ratios given in Table 1. For graphene platelets derived from graphite flakes and powder, the measured O/C ratios (~0.068 and 0.041, respectively) were among the lowest that have ever been reported for anodically exfoliated graphenes. This result could be reasonably anticipated, taking into account the short electrolysis time applied in both cases and the fact that the individual graphite particles were quickly detached from their pellet once they became exposed to the electrolyte solution, thus arresting their oxidation process. Nonetheless, such a limited extent of oxidation was attained at the expense of a comparatively low degree of platelet exfoliation, as noted above. The most enlightening results, though, were those obtained for graphene samples derived from the HOPG and graphite foil materials. First, the oxidation degree of the

platelets was seen to increase with increasing electrolysis time. For example, the measured O/C atomic ratios were 0.055, 0.091 and 0.180 for samples derived from HOPG after 3, 15 and 60 min of electrolysis, respectively, even when highly exfoliated platelets were brought about in all cases. Second, and more significantly, for a given electrolysis time the graphene platelets obtained from graphite foil were considerably less oxidized than their HOPG-derived counterparts (e.g., O/C ratios of 0.058 vs. 0.091 and 0.110 vs. 0.180 for 15 and 60 min, respectively, of electrolysis). We note that in all cases the reported amounts of oxygen must have been necessarily introduced during the electrochemical treatment, because the O/C ratios measured for all the as-received graphite types were very small (<0.01).

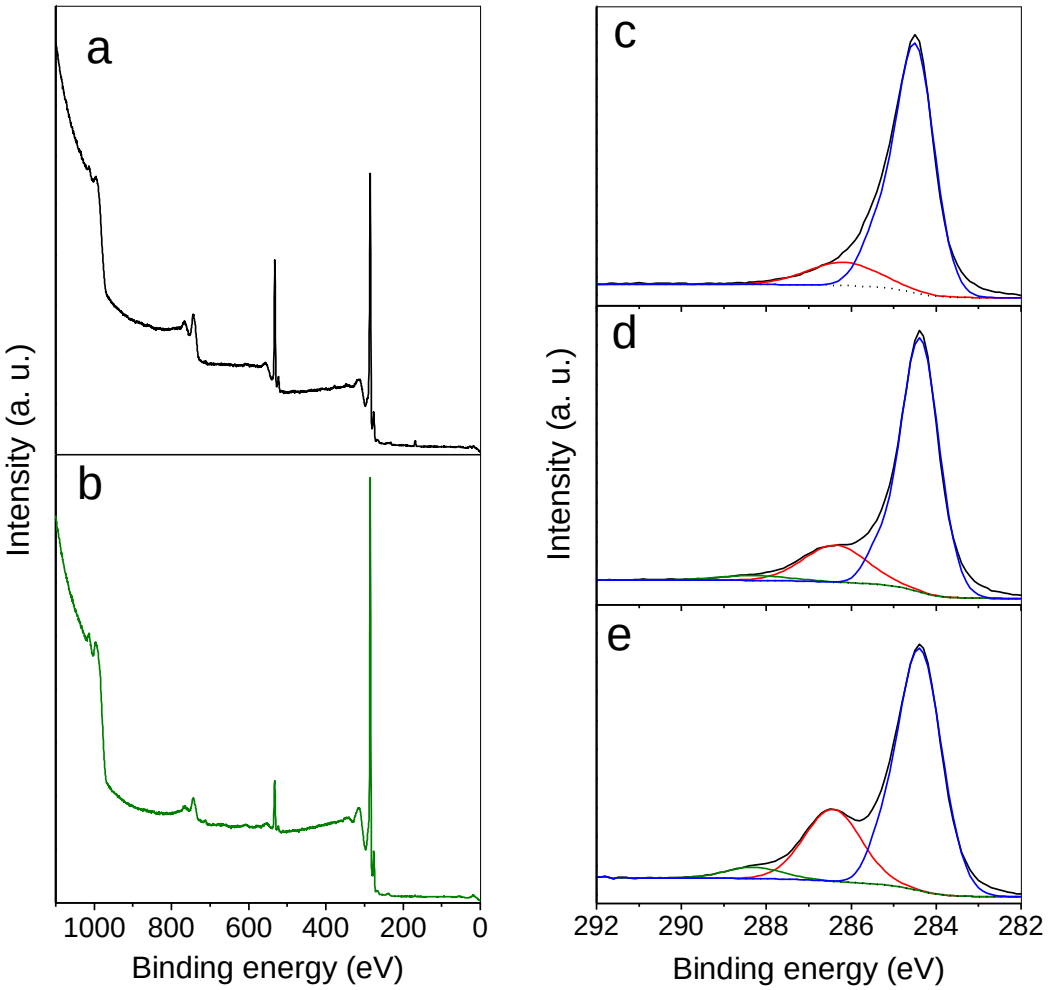

Figure 6. (a,b) Survey XPS spectra of anodically exfoliated graphenes obtained from (a) HOPG (60 min of exfoliation time) and (b) graphite powder (3 min). (c-e) High resolution core level C 1s spectra for graphenes obtained from graphite foil after 15 (c) and 60 (d) min of exfoliation time and (e) HOPG (60 min). In (c-e), components obtained by peak-fitting the experimentally obtained envelopes are indicated by blue, red and green traces.

Information on the specific types of oxygen functional groups generated upon exfoliation was gathered from the high resolution core level C 1s spectra of the samples, as illustrated in Fig. 6c-e for graphenes derived from graphite foil [15 (c) and 60 min (d) of electrolysis] and HOPG [60 min of electrolysis (e)]. The C 1s profiles were dominated by a peak located at ~284.6 eV, which can be ascribed to carbon atoms in unoxidized graphitic environments (C=C species), together with some additional components at higher binding energies that can be attributed to oxidized carbon atoms. More specifically, peak-fitting of these profiles yielded two components in addition to the main peak at 284.6 eV: one component was centered at about 286.5 eV, associated to C-O species (e.g., hydroxyl or epoxide groups) and the other one was located at ~288.0 eV, which can be assigned to C=O species (e.g., carbonyl groups) [51,56]. The high resolution C 1s spectra of the other graphene samples yielded the same components (results not shown), but as could be expected, it was generally observed that the weight of the C-O and C=O components relative to the main C=C graphitic peak tended to diminish as the O/C atomic ratio of the samples decreased. ATR-FTIR spectroscopy corroborated the presence of these oxygen functional groups, as exemplified in Fig. 7 for some of the graphene samples, derived from graphite powder [3 min of electrochemical exfoliation (a)], graphite foil [15 min (b) and 60 min (c)] and

HOPG [60 min (d)]. The following bands were observed for those samples with the highest O/C ratios: 3000-3500 cm^{-1} (O-H stretching vibrations from hydroxyl or carboxyl groups), ~1620 cm^{-1} (C=C stretching, skeletal vibrations from unoxidized graphitic domains) with a shoulder at about 1720 cm^{-1} (C=O stretching vibrations from carbonyl and carboxyl groups), 1300-1450 cm^{-1} (O-H bending vibrations and C-OH stretching vibrations from hydroxyl groups) with a shoulder/edge at ~1260 cm^{-1} (breathing vibrations from epoxy groups) and ~1070 cm^{-1} (C-O stretching in ethers or epoxides) [28,51,57]. Such bands were seen to strongly decline in intensity with decreasing O/C atomic ratio, and were barely discernible for graphene samples with the lowest O/C ratios [e.g., spectrum (a) in Fig. 7].

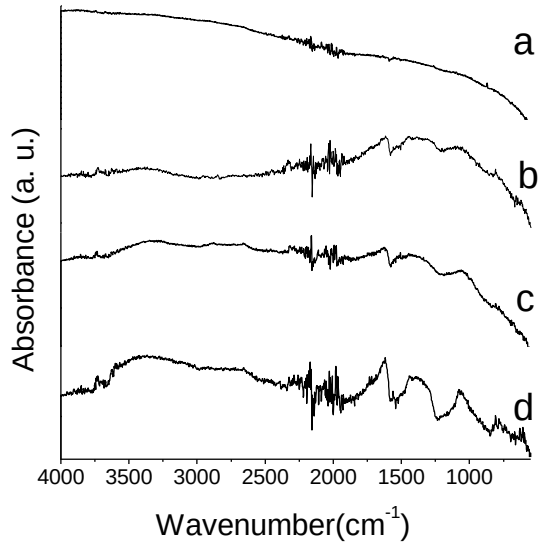

Figure 7. ATR-FTIR spectra of graphene samples obtained from (a) graphite powder (3 min of exfoliation time), (b) graphite foil (15 min), (c) graphite foil (60 min) and (d) HOPG (60 min).

As is well known from some chemically derived forms of graphene (i.e., GO and RGO) [9,11–13,50], oxidation is usually associated to the introduction of a significant amount of defects and structural imperfections in the carbon lattice of graphene sheets, which in turn has an impact on such relevant properties as their electrical conductivity. The structural quality of the anodically exfoliated graphenes was evaluated by means of Raman spectroscopy, as illustrated in Fig. 8 for some of the samples, specifically those derived from graphite powder [3 min (e)], graphite foil [15 min (f) and 60 min (g)] and HOPG [60 min (h)]. The Raman spectra of the starting graphite materials are shown in Fig. 8a-d as a reference. The first-order region of the spectra (1100-1700 cm^{-1}) comprised three peaks with different relative intensities depending on the specific sample: a strong peak located at about 1582 cm^{-1}, the so-called graphitic G band, which is the only band present in completely defect-free graphite/graphene, and two defect-related bands, D and D´, which appear at ~1350 and 1620 cm^{-1}, respectively [58–60]. The starting graphites were seen to have increasing structural quality in the following order: graphite powder, flakes, foil and HOPG. This was numerically reflected in the integrated intensity ratio of the D and G bands (I_D/I_G ratio), which is widely adopted as a quantitative measure of the amount of defects present in graphitic structures [59,60]. Indeed, the I_D/I_G ratios for the starting graphites were 0.10, 0.02, 0.01 and 0, respectively, in the order given above. Generally speaking, the Raman spectra of the graphene samples revealed that the D and D´ bands were typically more intense for those possessing higher O/C ratios, which can be generally taken as a clear indication of their larger extent of structural disorder. The calculated I_D/I_G values of the different graphene samples are given in Table 1, and contrast with the comparatively smaller values obtained for the starting graphites. There were, however, some exceptions to the direct correlation between O/C atomic ratio and I_D/I_G value. For instance, the I_D/I_G ratio

measured for graphene obtained by 60 min of electrolysis from HOPG was similar (slightly smaller) that that of the sample prepared by 15 min of electrolysis (1.23 vs. 1.35), even though the O/C ratio was much higher for the former (0.180 vs. 0.091). This result could be due to the fact that, above a certain defect density in the graphene/graphite lattice (in our case, defects are assumed to be mostly generated by oxygen groups covalently attached to carbon atoms), the intensity of the D band decreases, rather than increases, with increasing disorder [59,60]. Likewise, the spatial distribution of the defects, and not just their overall density, is known to have a bearing on the D band intensity, so that, e.g., a graphene sheet with scattered defects can yield a very different I_D/I_G value compared to that obtained for a sheet where the defects are closely aggregated, even though the overall defect density is the same in both cases [60]. This point could tentatively explain why graphene samples from different graphite types but having similar O/C ratios gave rather different I_D/I_G values in some cases: we speculate that the spatial distribution of their oxygen functional groups, and consequently of their defects, could be affected by the specific type of graphite used.

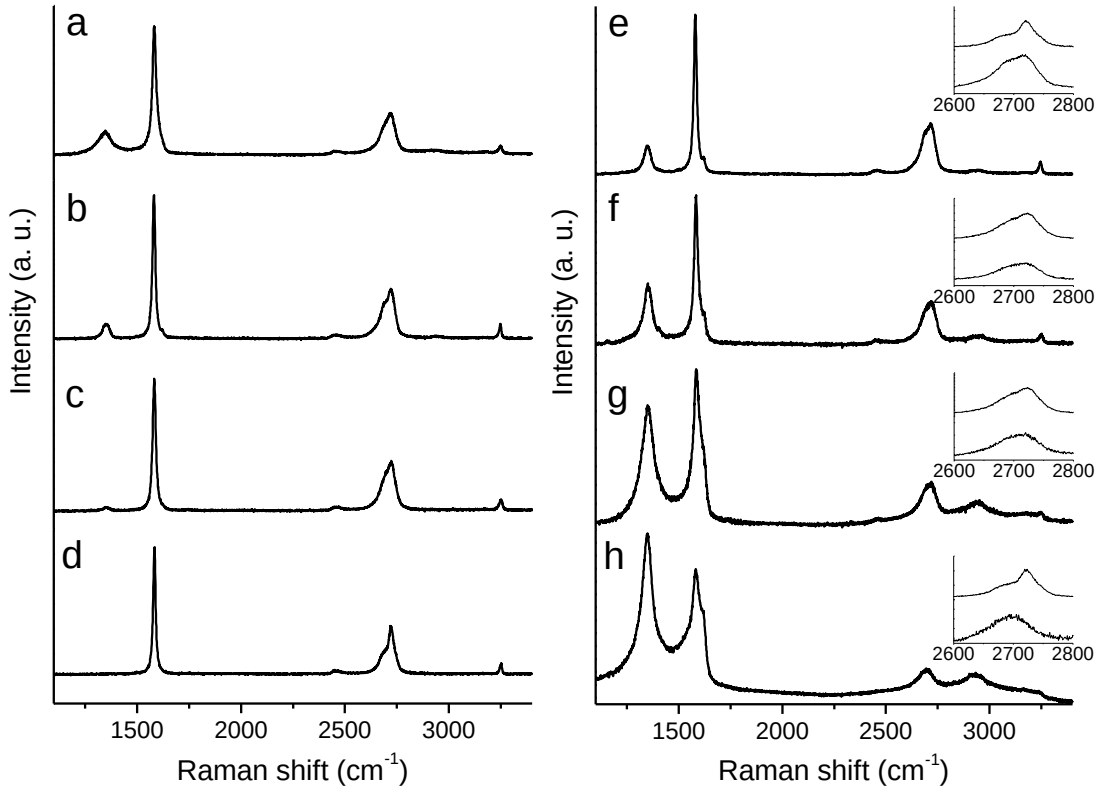

Figure 8. Raman spectra of (a) graphite powder, (b) graphite flakes, and (c) graphite foil, and of (d) HOPG, as well as Raman spectra of graphene samples obtained from (e) graphite powder (3 min of exfoliation time), (f), graphite foil (15 min), (g) graphite foil (60 min) and (h) HOPG (60 min). In the insets, magnified G´ band range for corresponding sample (lower trace) and its parent, non exfoliated graphite (upper trace).

The second-order region of the Raman spectra (2300-3300 cm^{-1}) was dominated by the G´ (or 2D) band, located at about 2700 cm^{-1}. As previously documented in the literature [58] and noticed here from the plots shown in the different insets to Fig. 8e-h, the shape of the G´ band for high quality graphites in bulk, non-exfoliated form was markedly asymmetrical (upper trace in each of the insets). By contrast, this band became more symmetrical and was slightly down-shifted upon anodic exfoliation to yield the different graphene samples (lower trace in the inset plots). Such features were consistent with these samples being comprised of few- to several-layered sheets [16,59–61], which in turn was in general agreement with the results obtained by AFM and discussed above (Fig. 5).

The starting graphites possess high electrical conductivity values, namely, 1.69×10^6 S m^{-1} in the case of HOPG and 9.84×10^4 S m^{-1} in that of graphite foil. The significant difference in conductivity between these two types of graphite derives from their distinct morphology (see Fig. 1a and 1c, and Fig. 2) and structural quality (Fig. 8c and 8d). Indeed, the already mentioned abundant folds, overlaps and wrinkles present in the platelets of graphite foil must act as dispersion sites for charge carriers, which would limit its conductivity. The electrical conductivity of the graphene samples after their processing into free-standing, paper-like films by vacuum filtration of the corresponding FMN-stabilized aqueous dispersions was also determined, and the results are listed in

Table 1. The conductivities of the graphene samples are notably lower than those of their corresponding parent graphites, being dominated by the relatively smaller size of their nanosheets and their relatively high content in oxygen. As could be expected, graphenes with lower O/C and I_D/I_G ratios, and therefore with smaller amounts of structural disorder, tended to be more electrically conductive. Values between ~4000 and 57000 S m^{-1} were measured, which compare favorably with those reported beforehand for other (non-annealed) anodically exfoliated graphenes (4000-25000 S m^{-1}) [29,31,56] and also for high quality graphenes prepared by direct exfolitation of graphite in the aqueous phase using sonication or shear-mixing and colloidally stabilized by surfactants (2000-5000 S m^{-1}) [48,62,63]. We attribute such a positive outcome not only to the relatively low defect content of some of our graphene samples, but also to the fact that FMN was used as a dispersant. It has just been demonstrated that small amounts of this vitamin B_2 derivative are able to colloidally stabilize large quantities of graphene flakes, so that the electrical conductivity of films obtained therefrom is not very significantly degraded by the use of this dispersant, contrary to the case of many surfactants investigated before [45].

The previous results comparing the characteristics of graphene nanosheets derived from different types of graphite are significant in that they suggest that the oxidation degree of the nanosheets can be minimized to a relevant extent simply by a proper choice of the graphite type. This finding would constitute an important asset in the anodic preparation of graphene, which has been regarded of relatively limited utility (compared to, e.g., cathodic exfoliation approaches) in the pursuit of high quality materials as a result of its extensive introduction of oxygen and related structural defects [17–19]. More to the point, the present results indicate that graphene nanosheets obtained from graphite foil are significantly less oxidized than their HOPG-derived

counterparts (see Table 1), even though they are prepared under exactly the same conditions and exhibit the same (high) degree of exfoliation. For instance, the O/C ratio of graphene obtained by 15 min of electrolysis of graphite foil was as low as 0.058, compared with 0.091 for its HOPG-derived equivalent, the former figure being similar to, or even lower than, the values that have been reported for many cathodically exfoliated graphenes [21–24,64,65]. Another advantage of using graphite foil vs. HOPG lies in its much lower price (~$0.1 per gram compared with ~$100 per gram for HOPG).

There still remains the question of why the HOPG and graphite foil materials led to graphene samples with so different degrees of oxidation and structural disorder, considering that both starting graphites were essentially devoid of heteroatoms, oxygen in particular, and defects (as judged by XPS and Raman spectroscopy). We believe that the nanometer- and/or micrometer-scale morphology of the graphite pieces has some influence on their exfoliation process. According to earlier reports [27,31], the anodic exfoliation of graphite in aqueous electrolytic solution proceeds through the following steps: (i) Hydroxyl and oxygen radicals are generated at the graphite anode by the oxidation of water molecules. The anode is then attacked by these radicals, initially at the highly reactive edge sites, leading to an initial expansion of the graphite layers from their edges. (ii) The oxidative expansion of the layer edges facilitates the intercalation of anions from the electrolyte (SO_4^{2-} in our case). These anions can subsequently decompose to give gaseous species (e.g., SO_2), which force the graphite layers apart, leading to their exfoliation. Thus, for HOPG, which is made up of perfectly packed layers with little or no voids in between, we interpret that a sizable intercalation of anions to prompt an effective exfoliation should heavily rely on the oxidation step to open up the layers at their edges and allow the anions in. This inevitably leads to a significant oxidation of the resulting graphene flakes. On the other hand, graphite foil is

produced by roll compaction of expanded graphite particles; thus, we can expect it to be riddled with voids and packing imperfections, as was indeed evident from the recorded FE-SEM and AFM images (e.g., Fig. 1c and 2b). Such pre-formed voids would facilitate the direct penetration of anions into this material without requiring some preliminary oxidation of the graphite layers. As a result, exfoliation of the graphite foil could be readily completed with a limited extent of oxidation compared to the case of HOPG, which would be much more dependent on oxidation for its exfoliation to proceed.

3.3. Biocompatibility of anodically exfoliated graphene films towards the L-929 cell line

Finally, graphene and graphene-based materials are currently the focus of increasing research attention regarding their potential application in biomedicine [4,66,67]. For example, graphene and graphene-containing (bio)polymer films could be used as substrates for cell growth and differentiation or tissue regeneration, with a high biocompatibility of such films being an obvious and necessary pre-requisite. Although previous studies have revealed GO, RGO and CVD-derived graphene substrates to be generally biocompatible towards a number of human and animal cell lines [66–70], to the best of our knowledge no biocompatibility studies are available for electrochemically exfoliated graphenes in general and anodically exfoliated graphenes in particular. Because the latter can be prepared with different physicochemical characteristics (e.g., a range of oxygen and defect contents, as shown above), which in turn can differ significantly from those of GO, RGO and CVD-derived graphene, it is unclear that the results of biocompatibility tests for these types of graphene can be generalized to anodically exfoliated graphenes. Hence, we carried out a preliminary biocompatibility assessment for thin films of several of the graphene samples prepared

in this work towards the murine fibroblast cell line L-929. This cell line is commonly employed in the cytotoxicity screening of prospective biomaterials [71], and has already been tested on a number of graphene-based and other carbon substrates [72–78]. The biocompatibility tests were accomplished on thin graphene films deposited from their corresponding FMN-stabilized aqueous dispersions onto polystyrene culture plates. FMN is an innocuous and safe biomolecule used as a food additive, and therefore constitutes an a priori very attractive dispersant of graphene sheets with a view to bio-related applications of this material [45].

The results of the L-929 cell viability tests for several graphene samples, based on the MTT assay and performed 1, 4 and 7 days after cell seeding on ~1 and 2 μm thick graphene films, are summarized in Fig. 9a, b and c, respectively. For comparison purposes, tests were also carried out on thin GO films obtained from aqueous dispersions that were either free of FMN and any other stabilizer (positive control) or incorporated about the same amount of FMN as that present in the dispersions of anodically exfoliated graphenes (~5 wt. % relative to the graphene content), as well as on the bare culture plates (negative control). The GO dispersions were prepared by oxidation of graphite powder via the Hummers method as described previously [51,52]. In general terms, all the anodically exfoliated graphenes afforded good cell proliferation rates, implying that they are highly biocompatible materials. After 7 days (Fig. 9c), cell proliferation was conspicuously higher for all the graphene samples (including the two GO specimens) compared with the bare culture plate. There were not large differences between the 1 and 2 μm thick films or between the different graphene samples, although some subtle trends could be noticed. For example, comparison of the three graphene samples obtained from HOPG with different exfoliation times (see Table 1) suggested cell proliferation after both 4 and 7 days to increase somewhat with increasing oxygen

content of the flakes. This observation would be consistent with the idea that hydrophilic surfaces tend to be better substrates for cell growth because they favour the cell-material interaction [73,79]. Such an effect appeared to be most obvious for the intermediate testing time of 4 days (Fig. 9b), with the highest cell proliferation being detected on the extensively oxidized, and thus more hydrophilic, GO samples (O/C atomic ratios ~0.40-0.45) and the lowest proliferation occurring on the less oxidized and hence more hydrophobic graphenes (e.g., the sample derived from graphite powder). However, factors other than oxygen content/hydrophilicity are also thought to play a role in the promotion of L-929 cell growth on carbon substrates, in particular their electrical conductivity (more conductive substrates allowing for higher proliferation of L-929 cells) [78]. Thus, the fact that the anodically exfoliated graphenes afforded highly conductive films while GO is an electrical insulator could help to explain why cell proliferation on the former eventually caught up with that on GO films after a 7 day period.

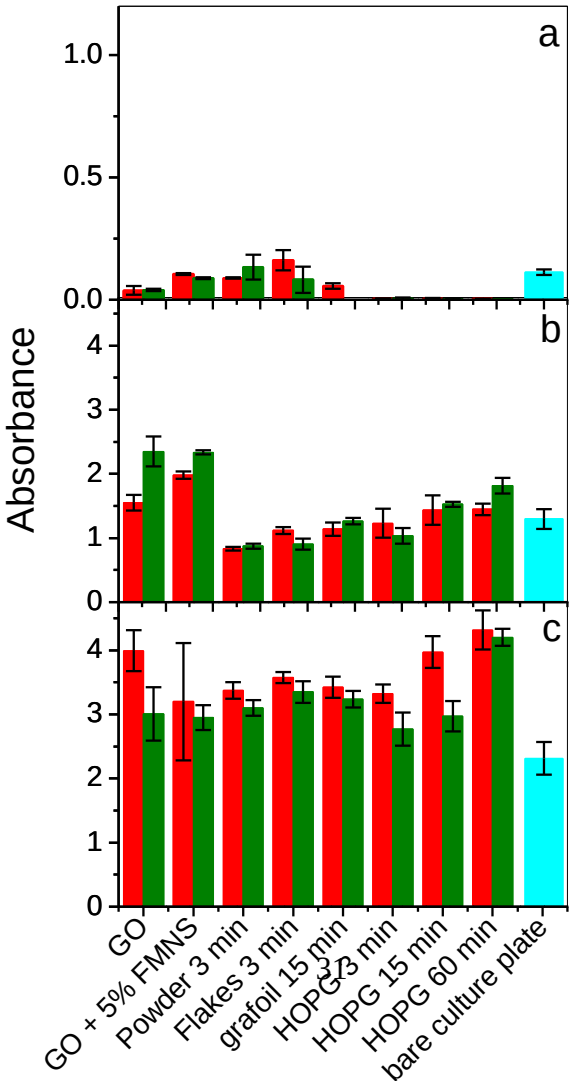

Figure 9. Results of L-929 cell proliferation tests, based on the MTT assay, for thin films of different anodically exfoliated graphenes, as well as GO, deposited from their corresponding aqueous dispersions onto polystyrene culture plates. The anodically exfoliated graphene dispersions used for the tests were colloidally stabilized in water by FMN molecules (FMN/graphene mass ratio of ~0.05), whereas GO dispersions both in the absence and presence of FMN were assessed. Red and green bars indicate ~1 and 2 μm thick films, respectively. The light blue bars correspond to tests performed on the bare culture plate. Results of the MTT assay 1 (a), 4 (b) and 7 (c) days after L-929 cell seeding are shown.

4. Conclusions

We have demonstrated that anodically exfoliated graphenes exhibiting a range of oxygen and defect contents can be attained through the use of starting graphite materials of different characteristics. Significantly, graphene nanosheets with high structural quality and minimized amount of oxygen functional groups (e.g., O/C atomic ratios of ~0.04-0.06) could be obtained by selecting appropriate types of graphite, such as graphite foil. This result was rationalized in terms of the specific microstructure of the starting graphite material and the exfoliation mechanism that is thought to be in place during the anodic process, and provides an avenue to access graphenes of similar quality to that achieved with cathodic exfoliation approaches, while avoiding the use of organic solvents at the same time. The implementation of anodically exfoliated graphenes in a range of potential uses could benefit from the ability to control their extent of oxidation and disorder. For example, graphenes with high oxygen/defect content would be suitable for the nucleation and growth of nanoparticles to produce hybrids for catalytic and biomedical applications, whereas the use of high quality materials would be

preferable when good electrical conductivity is required. Irrespective of their oxygen and defect content, the anodically exfoliated graphenes were seen to be highly biocompatible when processed into thin films from their corresponding aqueous dispersions stabilized by the innocuous and safe biomolecule flavin mononucleotide, as determined by cell proliferation tests performed with murine fibroblasts (L-929 line). Finally, the fact that the oxidation degree of anodically exfoliated graphene can be controlled (minimized) by means of some process variables (e.g., graphite type in the present case) suggests that other strategies could also be effective in the pursuit of very high quality nanosheets based on the aqueous anodic approach, and therefore they will be worth exploring in the future.

Acknowledgements

Financial support from the Spanish MINECO and the European Regional Development Fund (projects MAT2011-26399) is gratefully acknowledged. The authors also acknowledge partial funding of this work by Plan de Ciencia, Tecnología e Innovación 2013-2017 del Principado de Asturias and European Regional Development Fund through project GRUPIN14-056. M.A.-V. thanks the receipt of a pre-doctoral contract (FPI) from MINECO.

References

[1] Novoselov KS, Geim AK, Morozov SV, Jiang D, Zhang Y, Dubonos SV, et al. Electric field effect in atomically thin carbon films. Science 2004; 306: 666-9.

[2] Novoselov KS, Fal´ko VI, Colombo L, Gellert PR, Schwab MG, Kim K. A roadmap for graphene. Nature 2012; 490: 192-200.

[3] Randviir EP, Brownson DAC, Banks CE. A decade of graphene research: production, applications and outlook. Mater Today 2014; 17(9): 426-32.

[4] Ferrari AC, Bonaccorso F, Fal'ko VI, Novoselov KS, Roche S, Bøggild P et al. Science and technology roadmap for graphene, related two-dimensional crystals, and hybrid systems. Nanoscale 2015; 7: 4598-810.

[5] Bonaccorso F, Lombardo A, Hasan T, Sun Z, Colombo L, Ferrari AC. Production and processing of graphene and 2d crystals. Mater Today 2012; 15: 564-89.

[6] Zhang Y, Zhang L, Zhou C. Review of Chemical Vapor Deposition of Graphene and Related Applications. Acc Chem Res 2013; 46(10): 2329-39.

[7] Cai M, Thorpe D, Adamson DH, Schniepp HC. Methods of graphite exfoliation. J Mater Chem 2012; 22: 24992-5002.

[8] Zhong YL, Tian Z, Simon GP, Li D. Scalable production of graphene via wet chemistry: progress and challenges. Mater Today 2015; 18(2): 73-8.

[9] Park S, Ruoff RS. Chemical methods for the production of graphenes. Nat Nanotech 2009; 4: 217-24.

[10] Dreyer DR, Park S, Bielawski CW, Ruoff RS. The chemistry of graphene oxide. Chem Soc Rev 2010; 39: 228-40.

[11] Mattevi C, Eda G, Agnoli S, Miller S, Mkhoyan KA, Celik O, et al. Evolution of Electrical, Chemical, and Structural Properties of Transparent and Conducting Chemically Derived Graphene Thin Films. Adv Funct Mater 2009; 19(16): 2577-83.

[12] Rozada R, Paredes JI, Villar-Rodil S, Martínez-Alonso A, Tascón JMD. Towards full repair of defects in reduced graphene oxide films by two-step graphitization. Nano Res 2013; 6(3): 216-33.

[13] Rozada R , Paredes JI, López MJ, Villar-Rodil S, Cabria I, Alonso JA et al. From graphene oxide to pristine graphene: revealing the inner workings of the full structural restoration. Nanoscale 2015; 7: 2374-90.

[14] Coleman JN. Liquid exfoliation of defect-free graphene. Acc Chem Res 2013; 46(15): 14-22.

[15] Ciesielski A, Samorì P. Graphene via sonication assisted liquid-phase exfoliation. Chem Soc Rev 2014; 43: 381-98.

[16] Paton KR, Varrla E, Backes C, Smith RJ, Khan U, O'Neill A, et al. Scalable production of large quantities of defect-free few-layer graphene by shear exfoliation in liquids. Nature Mater 2014; 13: 624-30.

[17] Low CTJ, Walsh FC, Chakrabarti MH, Hashim MA, Hussain MA. Electrochemical approaches to the production of graphene flakes and their potential applications. Carbon 2013; 54: 1-21.

[18] Salavagione HJ. Promising alternative routes for graphene production and functionalization. J Mater Chem A 2014; 2: 7138-46.

[19] Abdelkader AM, Cooper AJ, Dryfe R, Kinloch IA. How to get between the sheets: a review of recent works on the electrochemical exfoliation of graphene materials from bulk graphite. Nanoscale 2015; 7, 6944-56.

[20] Wang J, Manga KK, Bao Q, Loh KP. High-yield synthesis of few-layer graphene flakes through electrochemical expansion of graphite in propylene carbonate electrolyte. J Am Chem Soc 2011; 133(23): 8888-91.

[21] Zhou M, Tang J, Chg Q, Xu G, Cui P, Qin LC. Few-layer graphene obtained by electrochemical exfoliation of graphite cathode. Chem Phys Lett 2013; 572: 61-5.

[22] Abdelkader AM, Kinloch IA, Dryfe RAW. Continuous electrochemical exfoliation of micrometer-sized graphene using synergistic ion intercalations and organic solvents. ACS Appl Mater Interfaces 2014; 6(3): 1632-9.

[23] Cooper AJ, Wilson NR, Kinloch IA, Dryfe RAW. Single stage electrochemical exfoliation method for the production of few-layer graphene via intercalation of tetraalkylammonium cations. Carbon 2014; 66: 340-50.

[24] Zhao M, Guo XY, Ambacher O, Nebel CE, Hoffmann R. Electrochemical generation of hydrogenated graphene flakes. Carbon 2015; 83: 128-35.

[25] Morales GM, Schifani P, Ellis G, Ballesteros C, Martínez G, Barbero C, et al. High-quality few layer graphene produced by electrochemical intercalation and microwave-assisted expansion of graphite. Carbon 2014; 49: 2809-16

[26] Liu N, Luo F, Wu H, Liu Y, Zhang C, J. Chen. One-step ionic-liquid-assisted electrochemical synthesis of ionic-liquid-functionalized graphene sheets directly from graphite. Adv Func Mater 2008; 18(10): 1518-25.

[27] Lu J, Yang J, Wang J, Lim A, Wang S, Loh KP. One-pot synthesis of fluorescent carbon nanoribbons, nanoparticles, and graphene by the exfoliation of graphite in ionic liquids. ACS Nano 2009; 3(8): 2367-75.

[28] Su CY, Lu AY, Xu Y, Chen FR, Khlobystov AN, Li LJ. High-quality thin graphene films from fast electrochemical exfoliation. ACS Nano 2011; 5(3): 2332-9.

[29] Parvez K, Li R, Puniredd SR, Hernandez Y, Hinkel F, Wang S, et al. Electrochemically exfoliated graphene as solution-processable, highly conductive electrodes for organic electronics. ACS Nano 2013; 7(4): 3598-606.

[30] Liu J, Yang H, Zhen SG, Poh CK, Chaurasia A, Luo J, et al. A green approach to the synthesis of high-quality graphene oxide flakes via electrochemical exfoliation of pencil core. RSC Adv 2013; 3(29): 11745-50.

[31] Parvez K, Wu ZS, Li R, Liu X, Graf R, Feng X, et al. Exfoliation of graphite into graphene in aqueous solutions of inorganic salts. J Am Chem Soc 2014; 136(16): 6083-91.

[32] Najafabadi AT, Gyenge E. High-yield graphene production by electrochemical exfoliation of graphite: Novel ionic liquid (IL)–acetonitrile electrolyte with low IL content. Carbon 2014; 71: 58-69.

[33] Rao KS, Sentilnathan J, Cho HW, Wu JJ, Yoshimura M. Soft processing of graphene nanosheets by glycine-bisulfate ionic-complex-assisted electrochemical exfoliation of graphite for reduction catalysis. Adv Funct Mater 2015; 25(2): 298-305.

[34] Liu J, Notarianni M, Will G, Tiong VT, Wang H, Motta N. Electrochemically exfoliated graphene for electrode films: effect of graphene flake thickness on the sheet resistance and capacitive properties. Langmuir 2013; 29(43): 13307-14.

[35] Lang FM, Magnier P, Action of oxygen and carbon dioxide above 100 millibars on "pure" carbon. In: Walker PA, editor. Chemistry and physics of carbon, vol 3, New York; Dekker; 1968 p. 121-209.

[36] Inagaki M, Kang F, Toyoda M. Exfoliation of graphite via intercalation compounds. Chem Phys Carbon 2004; 29: 1-69. In: Radovic LR, editor. Chemistry and physics of carbon, vol 29, New York; Dekker; 2004 p. 1-69.

[37] Vistica DT, Skehan P, Scudiero D, Monks A, Pittman A, Boyd MR. Tetrazolium-based assays for cellular viability: a critical examination of selected parameters affecting formazan production. Cancer Res 1991; 51: 2515-20.

[38] Chen K, Xue D. Preparation of colloidal graphene in quantity by electrochemical exfoliation. J Colloid Interface Sci 2014; 436: 41-6.

[39] Paredes JI, Martínez-Alonso A, Tascón JMD. Multiscale imaging and tip-scratch studies reveal insight into the plasma oxidation of graphite. Langmuir 2007; 23(17): 8932-43.

[40] Warner JH, Schäffel F, Rümmeli MH, Büchner B. Examining the edges of multi-layer graphene sheets. Chem Mater 2009; 21(12): 2418-21.

[41] Park S, An J, Jung I, Piner RD, An SJ, Li X, et al. Colloidal suspensions of highly reduced graphene oxide in a wide variety of organic solvents. Nano Lett 2009; 9(4); 1593-7.

[42] Villar-Rodil S, Paredes JI, Martínez-Alonso A, Tascón JMD. Preparation of graphene dispersions and graphene-polymer composites in organic media. J Mater Chem 2009; 19: 3591-3.

[43] Hernandez Y, Lotya M, Rickard D, Bergin SD, Coleman JN. Measurement of multicomponent solubility parameters for graphene facilitates solvent discovery. Langmuir 2010; 26(5): 3208-13.

[44] Yoon W, Lee Y, Jang H, Jang M, Kim JS, Lee HS, et al. Graphene nanoribbons formed by a sonochemical graphene unzipping using flavin mononucleotide as a template. Carbon 2015; 81: 629-38.

[45] Ayán-Varela M, Paredes JI, Guardia L, Villar-Rodil S, Munuera JM, Díaz-González M, et al. Achieving extremely concentrated aqueous dispersions of graphene flakes and catalytically efficient graphene-metal nanoparticle hybrids with flavin mononucleotide as a high-performance stabilizer. ACS Appl. Mater. Interfaces 2015; 7: 10293−307.

[46] Varrla E, Paton KR, Backes C, Harvey A, Smith RJ, McCauley J, et al. Turbulence-assisted shear exfoliation of graphene using household detergent and a kitchen blender. Nanoscale 2014; 6: 11810-9.

[47] Li D, Müller MB, Gilje S, Kaner RB, Wallace GG. Processable aqueous dispersions of graphene nanosheets. Nature Nanotech 2008; 3: 101-5.

[48] Guardia L, Fernández-Merino MJ, Paredes JI, Solís-Fernández P, Villar-Rodil S, Martínez-Alonso A, et al. High-throughput production of pristine graphene in an aqueous dispersion assisted by non-ionic surfactants. Carbon 2011; 49: 1653-62.

[49] Skoog DA, Holler FJ, Nieman TA, Principles of Instrumental Analysis, Hartcourt Brace & Company, Philadelphia, 1998, ch. 13.

[50] Erickson K, Erni R, Lee Z, Alem N, Gannett W, Zettl A. Determination of the local chemical structure of graphene oxide and reduced graphene oxide. Adv Mater 2010; 22(40): 4467-72.

[51] Fernández-Merino MJ, Guardia L, Paredes JI, Villar-Rodil S, Solís-Fernández P, Martínez-Alonso A, et al. Vitamin C is an ideal substitute for hydrazine in the reduction of graphene oxide suspensions. J Phys Chem C 2010; 114: 6426-32.

[52] Fernández-Merino MJ, Villar-Rodil S, Paredes JI, Solís-Fernández P, Guardia L, García R, et al. Identifying efficient natural bioreductants for the preparation of graphene and graphene-metal nanoparticle hybrids with enhanced catalytic activity from graphite oxide. Carbon 2013; 63: 30-44.

[53] Nemes-Incze P, Osváth Z, Kamarás K, Biró LP. Anomalies in thickness measurements of graphene and few layer graphite crystals by tapping mode atomic force microscopy. Carbon 2008; 46(11): 1435-42.

[54] Solís-Fernández P, Paredes JI, Villar-Rodil S, Martínez-Alonso A, Tascón JMD. Determining the thickness of chemically modified graphenes by scanning probe microscopy. Carbon 2010; 48: 2657-60.

[55] Gómez-Navarro C, Weitz RT, Bittner AM, Scolari M, Mews A, Burghard M, et al. Electronic transport properties of individual chemically reduced graphene oxide sheets. Nano Lett 2007; 7(11): 3499-503.

[56] Wu L, Li W, Li P, Liao S, Qiu S, Chen M, et al. Powder, paper and foam of few-layer graphene prepared in high yield by electrochemical intercalation exfoliation of expanded graphite. Small 2014; 10(7): 1421-9.

[57] Liu J, Poh CK, Zhan D, Lai L, Lim SH, Wang L, et al. Improved synthesis of graphene flakes from the multiple electrochemical exfoliation of graphite rod. Nano Energy 2013; 2(3): 377-86.

[58] Pimenta MA, Dresselhaus G, Dresselhaus MS, Cançado LG, Jorio A, Saito R. Studying disorder in graphite-based systems by Raman spectroscopy. Phys Chem Chem Phys 2007; 9: 1276-91.

[59] Saito R, Hofmann M, Dresselhaus G, Jorio A, Dresselhaus MS. Raman spectroscopy of graphene and carbon nanotubes. Adv Phys 2011; 60(3): 413-550.

[60] Ferrari AC, Basko DM. Raman spectroscopy as a versatile tool for studying the properties of graphene. Nature Nanotech 2013; 8: 235-46.

[61] Hao Y, Wang Y, Wang L, Ni Z, Wang Z, Wang R, et al. Probing layer number and stacking order of few-layer graphene by raman spectroscopy. Small 2010; 6(2): 195-200.

[62] De S, King PJ, Lotya M, O´Neill A, Doherty EM, Hernandez Y, et al. Flexible, transparent, conducting films of randomly stacked graphene from surfactant-stabilized, oxide-free graphene dispersions. Small 2010; 6(3): 458-64.

[63] Zhang L, Zhang Z, He C, Dai L, Liu J, Wang L. Rationally designed surfactants for few-layered graphene exfoliation: ionic groups attached to electron-deficient π-conjugated unit through alkyl spacers. ACS Nano 2014; 8(7): 6663-70.

[64] Huang H, Xia Y, Tao X, Du J, Fang J, Gan Y, et al. Highly efficient electrolytic exfoliation of graphite into graphene sheets based on Li ions intercalation–expansion–microexplosion mechanism. J Mater Chem 2012; 22: 10452-6.

[65] Najafabadi AT, Gyenge E. Synergistic production of graphene microsheets by simultaneous anodic and cathodic electro-exfoliation of graphitic electrodes in aprotic ionic liquids. Carbon 2015; 84: 449-59.

[66] Mao HY, Laurent S, Chen W, Akhavan O, Imani M, Ashkarran AA, et al. Graphene: promises, facts, opportunities, and challenges in nanomedicine. Chem Rev 2013; 113(5): 3407-24.

[67] Zhang H, Grüner G, Zhao Y. Recent advancements of graphene in biomedicine. J Mater Chem. B 2013; 1: 2542-67.

[68] Sanchez VC, Jachak A, Hurt RH, Kane AB. Biological interactions of graphene-family nanomaterials: an interdisciplinary review. Chem Res Toxicol 2012; 25(1): 15-34.

[69] Yang K, Li Y, Tan X, Peng R, Liu Z. Behavior and toxicity of graphene and its functionalized derivatives in biological systems. Small 2013; 9(9-10): 1492-503.

[70] Akhavan O, Ghaderi E, Abouei E, Hatamie S, Ghasemi E. Accelerated differentiation of neural stem cells into neurons on ginseng-reduced graphene oxide sheets. Carbon 2014; 66: 395-406.

[71] Biological evaluation of medical devices. Part 5: Tests for in vitro cytotoxicity. ISO 10993-5: 2009.

[72] Chen H, Müller MB, Gilmore KJ, Wallace GG, Li D. Mechanically strong, electrically conductive, and biocompatible graphene paper. Adv Mater 2008; 20(18): 3557-61.

[73] Yan X, Chen J, Yang J, Xue Q, Miele P. Fabrication of free-standing, electrochemically active, and biocompatible graphene oxide−polyaniline and graphene−polyaniline hybrid papers. ACS Appl Mater Interfaces 2010; 2(9): 2521-9.

[74] Fan H, Wang L, Zhao K, Li N, Shi Z, Ge Z, et al. Fabrication, mechanical properties, and biocompatibility of graphene-reinforced chitosan composites. Biomacromolecules 2010; 11(9): 2345-51.

[75] Sayyar S, Murray E, Thompson BC, Gambhir S, Officer DL, Wallace GG. Covalently linked biocompatible graphene/polycaprolactone composites for tissue engineering. Carbon 2013; 52: 296-304.

[76] Correa-Duarte MA, Wagner N, Rojas-Chapana J, Morsczeck C, Thie M, Giersig M. Fabrication and biocompatibility of carbon nanotube-based 3d networks as scaffolds for cell seeding and growth. Nano Lett 2004; 4(11): 2233-6.

[77] Lobo AO, Corat MAF, Antunes EF, Palma MBS, Pacheco-Soares C, Garcia EE, et al. An evaluation of cell proliferation and adhesion on vertically-aligned multi-walled carbon nanotube films. Carbon 2010; 48 (1): 245-54.

[78] Kim SI, Sahu BB, Kim SE, Ali A, Choi EH, Han JG. Controlling conductivity of carbon film for L-929 cell biocompatibility using magnetron sputtering plasmas. J Mater Chem B 2015; 3(16): 3267-78.

[79] Akhavan O, Ghaderi E. The use of graphene in the self-organized differentiation of human neural stem cells into neurons under pulsed laser stimulation. J Mater Chem B 2014; 2(34): 5602-11.